AGU PUBLICATIONS

Geophysical Research Letters

RESEARCH LETTER

10.1002/2016GL068279

**Key Points:**
- Evaluation of the EPP-induced $O_3$ variability on long time scales
- EPP causes an average upper stratospheric $O_3$ depletion of about 10–15% on a monthly basis
- Discrimination between EPP and solar irradiance effects on ozone

**Supporting Information:**
- Supporting Information S1

**Correspondence to:**
A. Damiani,
alecarlo.damiani@gmail.com

**Citation:**
Damiani, A., B. Funke, López Puertas, M., M. L. Santee, R. R. Cordero, and S. Watanabe (2016), Energetic particle precipitation: A major driver of the ozone budget in the Antarctic upper stratosphere, *Geophys. Res. Lett.*, *43*, 3554–3562, doi:10.1002/2016GL068279.

Received 15 FEB 2016
Accepted 22 MAR 2016
Accepted article online 29 MAR 2016
Published online 9 APR 2016
Corrected 9 MAY 2016

This article was corrected on 9 MAY 2016. See the end of the full text for details.



# Energetic particle precipitation: A major driver of the ozone budget in the Antarctic upper stratosphere

**Alessandro Damiani[1], Bernd Funke[2], Manuel López Puertas[2], Michelle L. Santee[3], Raul R. Cordero[4], and Shingo Watanabe[1]**

[1]Japan Agency for Marine-Earth Science and Technology, Yokohama, Japan, [2]Instituto de Astrofísica de Andalucía, CSIC, Granada, Spain, [3]Jet Propulsion Laboratory, California Institute of Technology, Pasadena, California, USA, [4]Physics Department, University of Santiago de Chile, Santiago, Chile

**Abstract** Geomagnetic activity is thought to affect ozone and, possibly, climate in polar regions via energetic particle precipitation (EPP) but observational evidence of its importance in the seasonal stratospheric ozone variation on *long time scales* is still lacking. Here we fill this gap by showing that at high southern latitudes, late winter ozone series, covering the 1979–2014 period, exhibit an average stratospheric depletion of about 10–15% on a monthly basis caused by EPP. Daily observations indicate that every austral winter EPP-induced low ozone concentrations appear at about 45 km in late June and descend later to 30 km, before disappearing by September. Such stratospheric variations are coupled with mesospheric ozone changes also driven by EPP. No significant correlation between these ozone variations and solar ultraviolet irradiance has been found. This suggests the need of including the EPP forcing in both ozone model simulations and trend analysis.

## 1. Introduction

In the 1980s the discovery of the so-called ozone hole [*Farman et al.*, 1985] in Antarctica underlined the effects of human activity on the environment and global change. Soon after, an international agreement to preserve the ozone ($O_3$) layer was signed, and the international community started accurate monitoring of atmospheric gases in order to evaluate the effectiveness of precautions taken. Nevertheless, since natural factors also influence $O_3$, they must be fully understood in order to assess the expected future $O_3$ recovery.

Among these natural factors, solar activity is known to affect the abundance of $O_3$ in the middle atmosphere in several ways. The wavelength dependence of the solar irradiance variation over both the 11 year and 27 day cycles can induce $O_3$ changes in phase with solar activity [*Hood et al.*, 2015]. The analysis of various long-term $O_3$ data sets has shown that the solar cycle (SC) amplitude of stratospheric $O_3$ is of a few percent. However, since these measurements are mainly based on solar occultation and backscatter instruments, they do not cover the dark winter high latitudes.

Limb sounders aboard polar-orbiting spacecraft can probe the winter night polar regions although these data sets usually extend to less than one SC. The energetic particle precipitation (EPP), which is directly or indirectly influenced by solar activity, has its major impact in the winter polar night. Thus, the limb sounders have a great advantage for understanding the influence of EPP on atmospheric composition, and $O_3$ in particular. EPP routinely impacts the polar regions, ionizes the atmosphere, and affects the neutral molecules by enhancing the concentration of odd nitrogen ($NO_x$) and odd hydrogen ($HO_x$) species. Thus, $O_3$ can be depleted by efficient $HO_x$ and/or $NO_x$-catalytic cycles [*Crutzen et al.*, 1975; *Solomon et al.*, 1981] during sporadic solar proton events (SPE) [*Jackman et al.*, 2001; *Funke et al.*, 2011; *López-Puertas et al.*, 2005] as well as during the occurrence of energetic electron precipitation (EEP) [*Verronen et al.*, 2011a] and by low-energy particles [*Randall et al.*, 2007; *Sinnhuber et al.*, 2014]. In particular, while SPE and EEP can directly affect the mesosphere (EPP-DE, direct effect), the (almost) continuous flux of lower energy precipitating electrons related to geomagnetic activity produces high $NO_x$ amounts in the upper mesosphere/thermosphere. Since $NO_x$ is chemically long lived in the absence of solar radiation, it can be transported downward during winter $NO_x$ inside the polar vortex by the residual circulation and thus influence stratospheric $O_3$ [*Callis et al.*, 1998; *Randall et al.*, 2005]. This so-called EPP-IE (indirect effect) is more important in the Antarctic than in the Arctic because the larger stability of the Antarctic vortex allows $NO_x$ to be transported deeper in the stratosphere [*Randall et al.*, 2007; *Funke et al.*, 2014; *Baumgaertner et al.*, 2009].

Previous simulations of the EPP-induced stratospheric $O_3$ depletion for the Antarctic showed decreases of up to about 20–40% under extreme geomagnetic conditions [*Baumgaertner et al.*, 2009; *Peck et al.*, 2015] and up to about 10% on average [*Semeniuk et al.*, 2011; *Rozanov et al.*, 2012]. Nevertheless, although this mechanism is thought to be a significant process in governing the $O_3$ budget and, potentially, the regional climate, observational evidence is still limited [*Callis et al.*, 1998; *Fytterer et al.*, 2015].

In order to fill this gap, this paper focuses on the analysis of the $O_3$ variability within the southern polar regions in response to solar/geomagnetic activity during the 1979–2014 period by combining satellite $O_3$ observations from Solar Backscatter Ultraviolet Radiometer (SBUV and SBUV/2) and Microwave Limb Sounder (MLS). In particular, we analyze the correlation of the $O_3$ variability with the geomagnetic conditions and with solar irradiance in an attempt to distinguish between the two effects and to quantify the $O_3$ variations caused by EPP on long time scales.

## 2. Data and Methods

We used version 3.3 (v.3.3) level 2 data of $O_3$ and $HNO_3$ from 2005 to 2014 from the NASA EOS (Earth Observing System) MLS aboard the Aura satellite [*Froidevaux et al.*, 2008; *Santee et al.*, 2007; *Livesey et al.*, 2013]. The vertical resolution of MLS $O_3$ data between the upper stratosphere and the lower mesosphere is about 2.5–4 km, while the precision of the individual $O_3$ profiles ranges from 0.1 to 0.5 ppmv, and the accuracy is about 5–20%. The vertical resolution of MLS $HNO_3$ data is about 3–5 km, the precision is 0.7–1.2 ppbv, and the accuracy ranges between 0.5 and 2 ppbv.

We also analyzed $O_3$ data measured by SBUV(/2) instruments for the 1979–2014 period. Recently, the data have been reprocessed based on the v8.6 retrieval algorithm with several improvements [*Bhartia et al.*, 2013; *Kramarova et al.*, 2013]. Here we used two different SBUV time series, based on different intersatellite calibration approaches (i.e., the SBUV MOD data set and the SBUV merged cohesive data set).

A multiple linear regression (MLR) analysis has been applied to MLS, SBUV MOD, and SBUV merged cohesive data. In addition to the usual predictors, the regression includes also a geomagnetic/EPP term. For the MLR of the MLS data we employed a monthly quasi-biennial oscillation term (i.e., zonal winds over Singapore at 10 and 30 hPa), an ENSO term (multivariate ENSO index), a solar term ($F_{10.7}$ index), a geomagnetic term (*Ap* or *AE* index), and a linear term as predictors. In order to account for the observed time lag introduced by vertical transport, below 0.5 hPa the geomagnetic index was weighted with the contribution of the preceding months (up to 3 months) as in a recent work [*Funke et al.*, 2014], while no lag was used for the upper altitudes. Note that the specific weight is slightly different for the early and late winter months and reflects the different descent rates and the altitude of the bulk of EPP-$NO_x$. Overall, this results in a stronger weight applied to both the current and the closest (farthest) preceding month for the early (late) winter period.

The MLR applied to SBUV data slightly differs in using the equivalent effective stratospheric chlorine instead of the linear term and in the additional inclusion of a volcanic term. Results are presented in percent per 13 *Ap* (204 *AE*) index units (which corresponds to the average of the investigated period) and 100 $F_{10.7}$ units. The autocorrelation of residuals of the various MLR analyses is corrected as in *Tiao et al.* [1990].

## 3. Results

Figure 1a shows the temporal evolution of the solar and geomagnetic activity during the 1979–2014 period. We employed the widely used $F_{10.7}$ index as a proxy of the solar irradiance variation and the *Ap* and *AE* indices as proxies of the geomagnetic/EPP activity. Both solar irradiance and geomagnetic activity are affected by the 11 year component of the solar activity [*Echer et al.*, 2004]. In particular, the peak of the geomagnetic activity typically follows the peak in the solar irradiance with a lag of about 1–2 years [*Echer et al.*, 2004; *Du*, 2011].

Figure 1b shows the temporal evolution of the recently developed *Ap*-based parameterization of the EPP-related $NO_y$ (total reactive nitrogen) amounts below 0.02 hPa within the southern polar vortex [*Funke et al.*, 2014] (EPP-$NO_y$) from April to September for the 1979–2014 period. Although EPP-$NO_y$ amounts peak in 1982, 1991, 2000, and 2003, with values reaching about 2.3 gigamole during the latter winter, we also note significant amounts of EPP-$NO_y$ in 2005, very low amounts particularly in 2008–2010, and then slightly higher values mostly for 2012 and 2013.

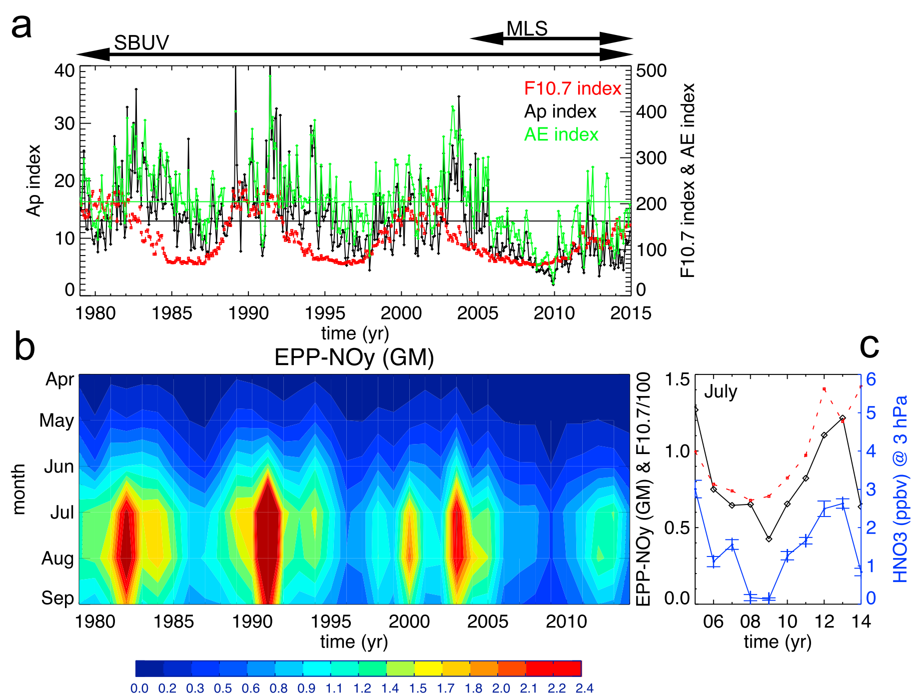


**Figure 1.** (a) Monthly temporal evolution of the *Ap* (black line), *AE* (green line), and $F_{10.7}$ (red line) indices during the 1979–2014 period. Horizontal lines show the average value for the investigated period. Horizontal lines with arrows show the time coverage of MLS and SBUV observations. (b) Temporal evolution of the parameterized monthly EPP-$NO_y$ amounts within the southern polar vortex from April to September for the 1979–2014 period. (c) Year-to-year variability of the EPP-$NO_y$ amounts (black line), the zonal mean at 3 hPa of MLS $HNO_3$ averaged over latitudes poleward of 70°S (blue line; for a meaningful visualization values have been reduced by 2 ppbv) and the $F_{10.7}$ index (red dashed line) in July for the 2005–2014 period.

While in the mesosphere $NO_x$ almost coincides with the total $NO_y$, in the upper stratosphere the conversion from $NO_x$ to other reservoirs must be taken into account. There, $NO_x$ is mainly converted to $N_2O_5$, $ClONO_2$, and $HNO_3$. Indeed, various studies reported winter stratospheric $HNO_3$ enhancements within the polar regions depending on the geomagnetic activity [*de Zafra and Smyshlyaev*, 2001; *Stiller et al.*, 2005; *Verronen et al.*, 2011b; *Orsolini et al.*, 2009]. Those authors pointed out that $HNO_3$ formation in the polar upper stratosphere requires a sufficient amount of $NO_x$ and is produced by heterogeneous chemistry on sulfate aerosols and/or by ion cluster chemistry via different paths. The latter, together with the presence of a significant amount of EPP-$NO_x$, is perhaps the most important factor for the investigated altitudes. Moreover, *Stiller et al.* [2005] proved that EPP-induced $HNO_3$ depends on the formation of $N_2O_5$ as an interim step and that nighttime conditions are essential for its production. Since the widely used Michelson Interferometer for Passive Atmospheric Sounding (MIPAS) $NO_y$ observations [*Funke et al.*, 2014] ends in early 2012, we also use MLS $HNO_3$ which is a good proxy for the odd nitrogen species. In Figure 1c we compare the parameterized EPP-$NO_y$ with the measured zonal mean $HNO_3$ at 3 hPa for latitudes poleward of 70°S in July for the period of MLS $HNO_3$ measurements (i.e., 2005–2014 years). Despite some minor discrepancies, the interannual variability of the EPP-$NO_y$ is generally close to the observed $HNO_3$ variability. As a further result we find that the EPP-$NO_y$ parameterization also gives a good prediction for the 2012–2014 winters when MIPAS $NO_y$ observations (on which the parameterization is based) are no longer available.

Since there are evident changes in EPP-$NO_y$ amounts during the austral winters of the 1979–2014 period (Figure 1b), it is reasonable to expect a corresponding modulation of $O_3$. Thus, we have applied a MLR analysis to the $O_3$ profiles retrieved from both SBUV and MLS instruments. As the intersatellite calibration is an important issue when dealing with SBUV data [*Tummon et al.*, 2015], two independent merged data sets, i.e., the SBUV MOD and SBUV merged cohesive data, have been considered. Moreover, since SBUV observations are available only for daytime conditions, we limited the analysis to August–September (Figure 2). The EPP signal is similar in both SBUV data sets and shows a significant and homogeneous $O_3$ reduction of about

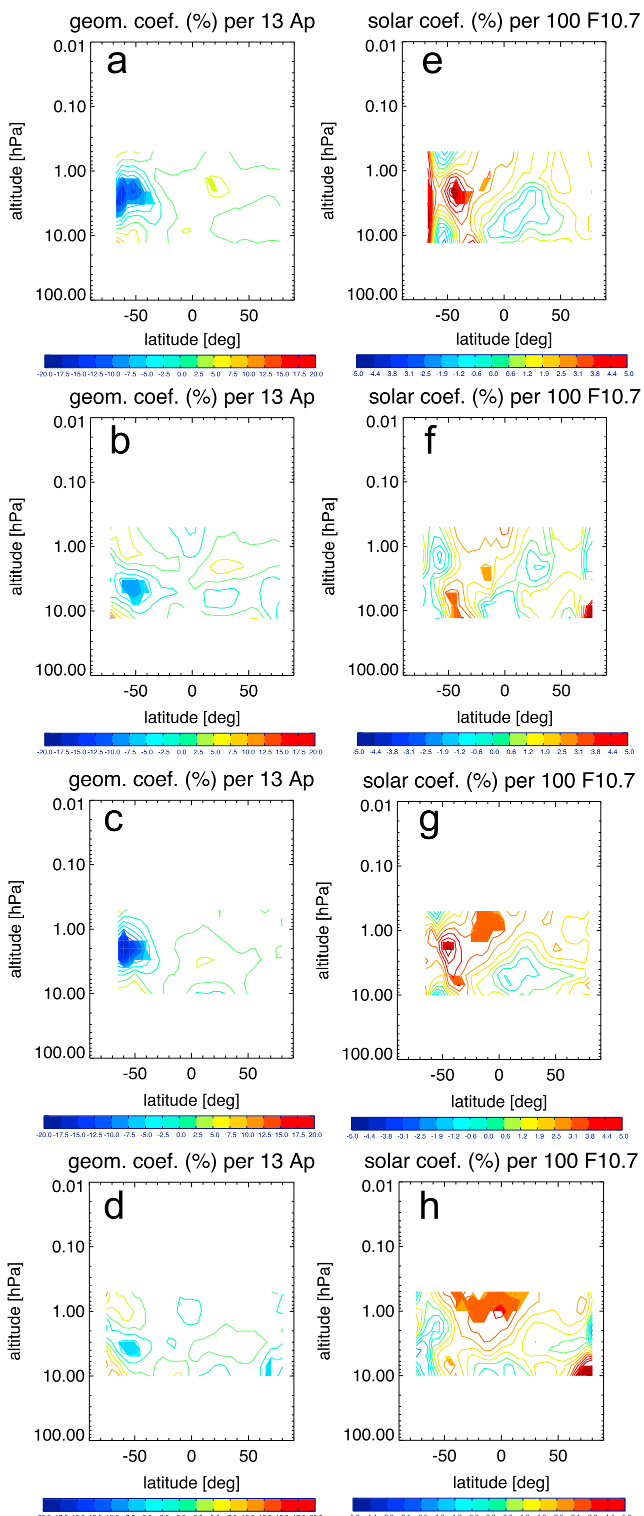


10–15% (Figures 2a and 2c) and 5–10% (Figures 2b and 2d) at latitudes poleward of about 50°S in August and September, respectively. In late winter, the upper stratospheric edge of the Southern polar vortex is usually located around 50–55°S [*Peck et al.*, 2015]. Therefore, the altitude of the peak of the $O_3$ response (2–3 hPa in August and 4–5 hPa in September) is consistent with the expected descent of the mesospheric $NO_x$-rich air down to the stratosphere. Moreover, Figures 2a and 2c suggest that even larger $O_3$ reduction could occur at latitudes poleward of about 70°S where the bulk of $NO_x$ is likely located.

On the other hand, the largest response of the solar UV coefficient appears at middle to low latitudes of the winter hemisphere (Figures 2e–2h) and suggests that photochemical processes as well as dynamical variability could play a role in determining such patterns [*Hood et al.*, 2015]. Indeed, we can expect the strongest solar response at low latitudes and in the summer hemisphere where the ozone is roughly in steady state, but both SBUV data sets show an overall stronger response at the middle latitudes of the winter hemisphere. One possible explanation of this apparent incongruence could be that solar UV variation can modulate also dynamical changes in the stratosphere [*Kodera and Kuroda*, 2002] although this hypothesis is still under discussion.

**Figure 2.** (a, b) Geographic distribution of the geomagnetic coefficient (per 13 *Ap* units, in percent) between 0.01 and 100 hPa as obtained by a multiple linear regression (MLR) based on SBUV MOD $O_3$ data in August (Figures 2a) and September (Figure 2b) for the 1979–2014 period (see text for details); (c, d) same as Figures 2a and 2b except using SBUV Merged Cohesive $O_3$ data as predictant; (e–h) same as Figures 2a–2d except showing the solar coefficient (per 100 $F_{10.7}$ units, in percent). Filled contours indicate statistical significance at the 2 sigma level. Note that because of the limited vertical resolution in the lower stratosphere/troposphere, data below about 10 hPa have not been used.

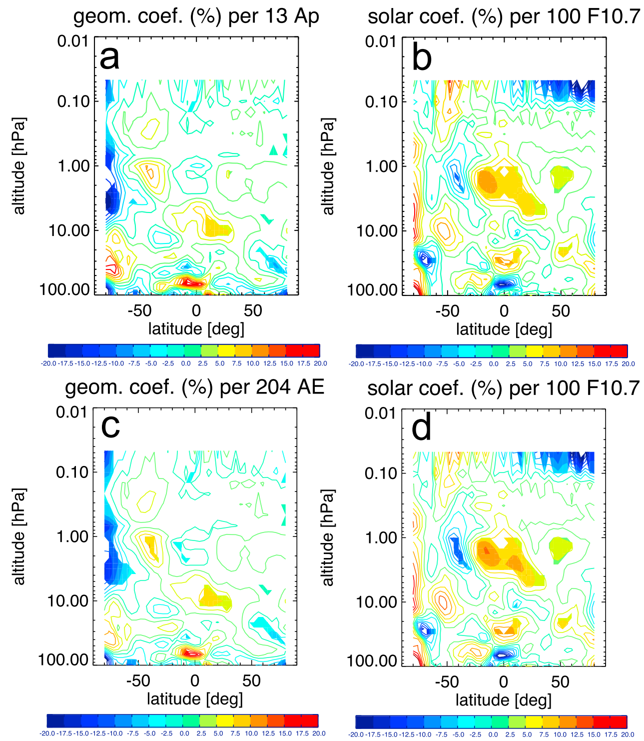


**Figure 3.** (a) Geographic distribution of the *Ap*-based geomagnetic coefficient (per 13 *Ap* units, in percent) between 0.01 and 100 hPa as obtained by a multiple linear regression based on MLS $O_3$ in May–September for the 2005–2014 period (see text for details); (b) same as Figure 3a except showing the solar coefficient (per 100 $F_{10.7}$ units, in percent); (c and d) same as Figures 3a and 3b except using an *AE*-based geomagnetic coefficient (shown in Figure 3c per 204 *AE* units, in percent) in the multiple linear regression. Filled contours indicate statistical significance at the 2 sigma level.

Because of its large temporal extension and the dense sampling at high latitudes, the SBUV data set is probably the best data set to investigate the seasonality of the ozone response; nevertheless, drift issues in the data sets could also potentially affect the reliability of this response [*Lean*, 2014]. The significant solar UV response at high southern latitudes (60–70°S) in the SBUV MOD data set (Figure 2e) is not present in the SBUV Merged Cohesive $O_3$ data set (Figure 2h). It is then not clear if it is a realistic feature or an artifact introduced in the merging of the data. This should be further investigated.

In order to take advantage of the MLS nighttime observations and due to the shortness of the data set, MLR has been applied to monthly $O_3$ data in May–September (Figure 3). Moreover, since MLS probes not only the stratosphere, where the $NO_x$-catalytic cycles dominate the $O_3$ loss, but also the mesosphere, where $O_3$ loss is controlled by the $HO_x$-catalytic cycles; in the following regression analysis we employed the weighted *Ap* index below 0.5 hPa (as in the previous analysis) while the actual *Ap* index for higher altitudes. In this way, we account for the direct impact of EPP (i.e., EPP-DE) and for the time needed to transport the air from the upper to the lower atmosphere (i.e., EPP-IE).

Figure 3a shows the geographic distribution of the geomagnetic coefficient between 0.01 and 100 hPa. Analogously to recent model results including the EPP forcing [*Rozanov et al.*, 2012], $O_3$ decrease (up to about 15 %) is evident in both the upper stratosphere and the mesosphere at latitudes poleward of 60–70°S, suggesting an EPP-induced effect there. While the mesospheric $O_3$ depletion is related to EPP-DE via $HO_x$-catalytic cycles, upper stratospheric changes are likely related to EPP-IE via descent of high $NO_x$ amounts produced at upper altitudes. Note that the larger equatorward extension of the region affected by EPP of Figure 2 in comparison to that showed in Figure 3 is mainly due to the different months included in the regression (i.e., only August or September for SBUV while May to September for MLS).

Moreover, it is interesting to note that similar results are obtained when the MLR includes the *AE* index, instead of the *Ap* index, as geomagnetic term (Figure 3c). In the latter case the amplitude of the response is somewhat smaller (larger) in the stratosphere (mesosphere) and slightly more statistically significant above 0.5 hPa.

Figures 3b and 3d are analogous to Figure 3a except for showing the solar coefficient. While at low/middle latitudes a UV-induced $O_3$ enhancement is evident, no statistically significant changes are present at very high southern latitudes. Moreover, the strong negative $O_3$ response in the summer mesosphere is mainly related to increased water vapor photolysis and consequent $HO_x$ production during high solar irradiance periods.

In order to give a more solid ground to these correlations, we examined in detail the temporal evolution of the EPP-induced $O_3$ and $HNO_3$ variability as well as their correlations for the 2005–2014 period.

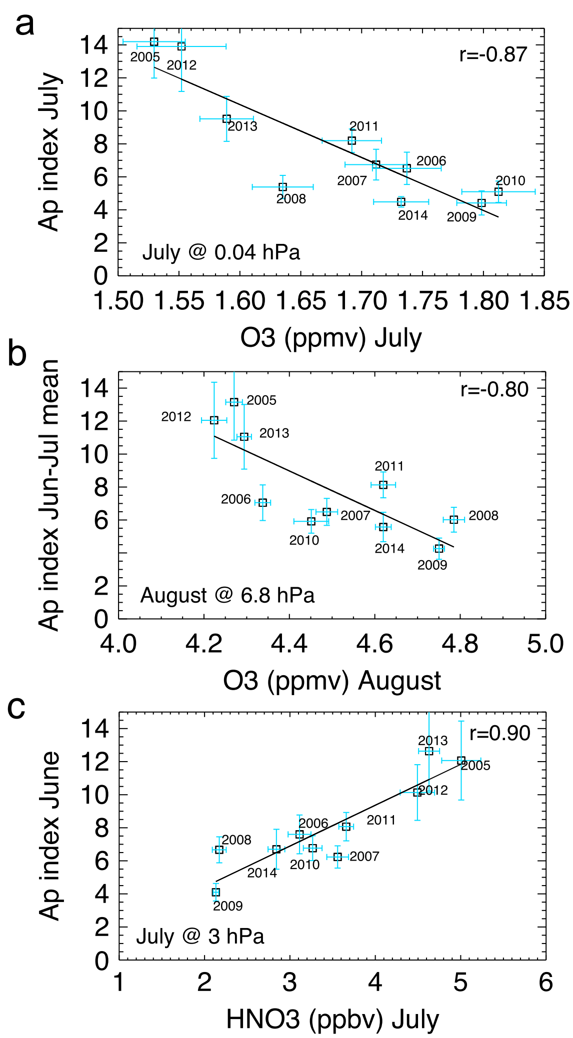


**Figure 4.** (a) Scatterplots between $O_3$ at 0.04 hPa and the *Ap* index for July, (b) $O_3$ at 6.8 hPa in August and the *Ap* index averaged over June and July, and (c) $HNO_3$ at 3 hPa in July and *Ap* index in June during the 2005–2014 period. $O_3$ and $HNO_3$ zonal means have been computed over latitudes poleward of 70°S (see text for details).

Under high geomagnetic activity conditions, polar $O_3$ can be depleted as a consequence of both medium- and low-energy precipitating electrons, which impact the middle/high mesosphere (above approximately 70 km) and the lower thermosphere, respectively. Therefore, we expect a prompt response of mesospheric $O_3$, which is directly influenced by EPP, but a delayed response of stratospheric $O_3$ due to the time required for the $NO_x$-rich air to descend from upper to lower altitudes. Figure 4 depicts the relationship between the geomagnetic *Ap* index and $O_3$ and $HNO_3$ zonal means averaged over latitudes poleward of 70°S (i.e., in the region not probed by SBUV observations) for July and August of the 2005–2014 period. Figure 4a presents a clear negative correlation ($r \sim 0.9$) between the *Ap* index and mesospheric $O_3$ (at 0.04 hPa, i.e., around the so-called tertiary ozone peak) in July. The years characterized by stronger geomagnetic activity (i.e., 2005, 2012, and 2013) show a reduced abundance of $O_3$, while increasing levels of $O_3$ along with decreasing levels of geomagnetic activity characterize the other years. Nighttime mesospheric $O_3$ depletion in polar regions under high geomagnetic activity has been reported before and ascribed to both sporadic SPEs [*Seppälä et al.*, 2006] and strong EEP events which can affect the composition of the mesosphere [*Andersson et al.*, 2014]. Both phenomena cause an additional ionization of the atmosphere, the production of high $HO_x$ mixing ratios and a consequent transient $O_3$ depletion [*Damiani et al.*, 2008]. Various SPEs able to affect these altitudes occurred mostly in July 2005 [*Damiani et al.*, 2010] while strong EEP events occurred in both 2005 and 2012 [*Andersson et al.*, 2014].

It is interesting to compare the mesospheric $O_3$ variability with the stratospheric $O_3$ changes caused by downward transport of upper mesospheric/thermospheric $NO_x$. Thus, Figure 4b shows the correlation between the $O_3$ zonal means at 6.8 hPa in August and the *Ap* index averaged over June and July (we take this averaged index to account for the time needed to transport the air from the lower thermosphere/mesosphere, where the EPP occur, to the stratosphere). As in Figure 4a, we note an intense $O_3$ depletion in 2005, 2012, and 2013, when the geomagnetic activity and EPP-$NO_y$ amounts are higher. On the other hand, record-high $O_3$ levels occur during 2008 and 2009, possibly because of the very low EPP-$NO_y$ amounts.

Because of the increasing solar illumination toward the end of the Antarctic winter, the EPP-induced enhancement in $HNO_3$ is mostly confined to July and the first half of August. Then, the vortex exposition to sunlight leads to fast photolysis of $HNO_3$ [*Stiller et al.*, 2005] and prevents its use as a proxy of EPP-induced odd nitrogen species. Therefore, Figure 4c shows the regression between the $HNO_3$ zonal mean at 3 hPa in July and the *Ap* index in June. The picture shows a positive correlation ($r = 0.9$) and is coherent with the expected high (low) EPP-$NO_y$ amounts during years with high (low) geomagnetic activity.

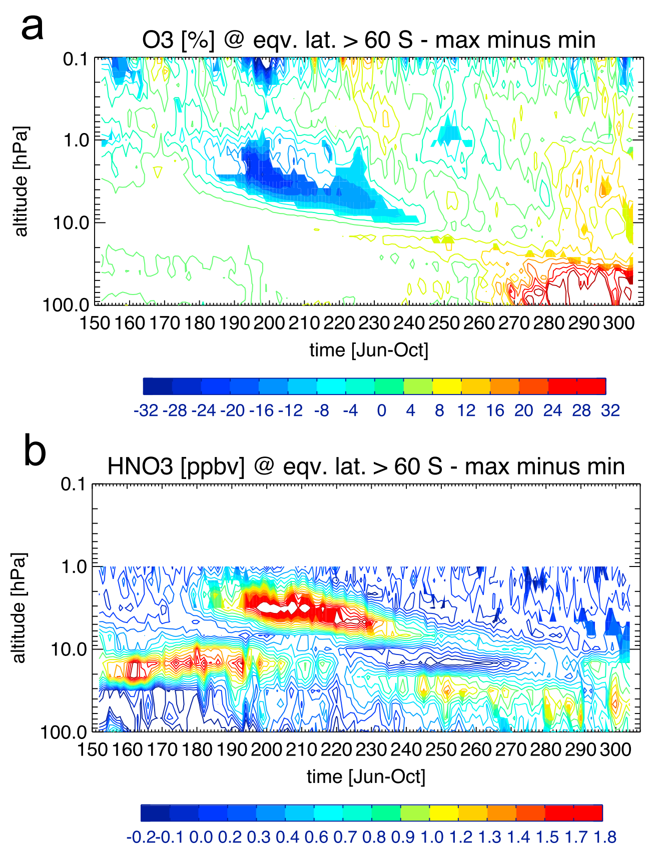


**Figure 5.** Differences in MLS (a) $O_3$ and (b) $HNO_3$ between the composite built by averaging the years characterized by high EPP-$NO_y$ (2005, 2012, 2013; maximum composite) and another one based on the remaining years (minimum composite) during the 2005–2014 period. Results are presented on a daily basis by computing the difference within the equivalent latitude of 60°S. Filled contours indicate statistical significance at the 2 sigma level.

In order to further examine the seasonal evolution of the EPP-induced effects on MLS $O_3$ and $HNO_3$, we build two composites by averaging the years characterized by high EPP-$NO_y$ (i.e., 2005, 2012, and 2013; maximum composite) and another based on the remaining years (minimum composite). To provide a vortex-centered view, Figure 5 shows the seasonal evolution of the $O_3$ and $HNO_3$ maximum-minimum differences in the zonal means computed within 60°S equivalent latitude [*Butchart and Remsberg*, 1986; *Manney et al.*, 2007] for the June–October period on a daily basis. In the stratosphere the amplitude of the daily differences peaks in July with changes up to about 20% and 2 ppbv in $O_3$ and $HNO_3$, respectively. $O_3$ changes start in June and then propagate to lower altitudes in July and August. No significant variations below 10 hPa occur in September. Similarly, enhancements in $HNO_3$ propagate from the upper to the middle stratosphere during the June–August period, after which incoming sunlight prevents that $NO_y$ descent in the form of $HNO_3$ in September.

Furthermore, although not shown here, a clear EPP signature in both $O_3$ and $HNO_3$ monthly data can be discerned also in the mesosphere (Figure S1 in the supporting information; note the increased $HNO_3$ between 1 and 0.1 hPa, likely caused by low-energy precipitating electrons, and the strong $O_3$ depletion above 0.1 hPa).

## 4. Discussion

Since EPP forcing is potentially able to affect polar climate, mostly via $O_3$ depletion [*Baumgaertner et al.*, 2009; *Semeniuk et al.*, 2011; *Rozanov et al.*, 2012; *Andersson et al.*, 2014], work is ongoing to include it within multi-model initiatives like Coupled Model Intercomparison Project Phase 6. Nevertheless, although some case studies have been reported [*Randall et al.*, 2005], definitive observational evidences on the importance of the EPP-$NO_x$ as an efficient modulator of $O_3$ over longer time scales are still lacking, and currently, the majority of CCMs still do not include this mechanism.

Here we showed that both MLS and SBUV observations at high southern latitudes present a clear response of stratospheric $O_3$ to EPP activity over solar cycle time scales. Overall, at high southern latitudes, the resulting $O_3$ depletion has been quantified at about 10–15 % on average. Nevertheless, the actual effects will depend also on the polar vortex dynamics which further can contribute to modulate the amount of $NO_y$ reaching the stratosphere.

On the other hand, the expected positive correlation between stratospheric $O_3$ and solar UV irradiance maximizes at middle latitudes possibly because solar UV modulates also dynamical changes [*Kodera and Kuroda*, 2002].

Detailed analysis based on MLS observations carried out on a daily basis shows negative (positive) $O_3$ ($HNO_3$) differences between years characterized by high and low geomagnetic activity and changes propagating from about 1 to 10 hPa during the June–September period. In particular, the winters of 2005, 2012, and 2013, which were characterized by stronger geomagnetic activity, showed the lower $O_3$ levels not only in the stratosphere, as expected due to EPP-$NO_x$ effects, but also in the mesosphere, where a direct impact of EPP has been recently reported to occur [*Andersson et al*., 2014], and this clearly points to a common geomagnetic origin of such changes.

In winter a negative latitudinal gradient in $O_3$ occurs because of the decrease with increasing latitude of the solar UV-induced $O_3$ production rate. Although the peaks of the solar and geomagnetic activity are somewhat lagged each other, on average the geomagnetic activity is higher around the solar maximum than around the solar minimum. Therefore, the latter, through the influence of the EPP-$NO_y$, would tend to further strengthen the $O_3$ gradient at high latitudes during solar maximum conditions. Additional modeling studies are necessary to assess to what degree these EPP-induced $O_3$ changes are actually able to influence the polar climate via temperature and wind perturbations.

Because $O_3$ variability in the upper polar stratosphere is mainly driven by chemistry, this region is commonly used for the detection of ozone hole recovery [*Miyagawa et al*., 2014]. The results of this study suggest that EPP-induced $O_3$ variations on a decadal time scale might be of importance in the analysis of upper stratospheric $O_3$ trends.

**Acknowledgments**
The present study was supported by the SOUSEI program, MEXT, JAPAN. The IAA team was supported by the Spanish MINECO under grant ESP2014-54362-P and EC FEDER funds. Work at the Jet Propulsion Laboratory, California Institute of Technology, was done under contract with NASA. The Chilean team was supported by FONDECYT (1140239). MLS/Aura data are available at the Jet Propulsion Laboratory MLS website: http://mls.jpl.nasa.gov/index.php. SBUV MOD data are available at http://acd-ext.gsfc.nasa.gov/Data_services/merged/, and SBUV merged cohesive data are available at ftp://ftp.cpc.ncep.noaa.gov/SBUV_CDR/. Zonal means computations within the equivalent latitudes or polar vortex edge are based on the derived meteorological products for MLS v3.3 data calculated from GEOS5-based Modern Era-Retrospective Analysis for Research and Applications (MERRA) reanalysis.

## References

Andersson, M. E., P. T. Verronen, C. J. Rodger, M. A. Clilverd, and A. Seppälä (2014), Missing driver in the Sun–Earth connection from energetic electron precipitation impacts mesospheric ozone, *Nat. Commun.*, doi:10.1038/ncomms6197.

Baumgaertner, A. J. G., P. Jöckel, and C. Brühl (2009), Energetic particle precipitation in ECHAM5/MESSy1—Part 1: Downward transport of upper atmospheric $NO_x$ produced by low energy electrons, *Atmos. Chem. Phys.*, *9*, 2729–2740, doi:10.5194/acp-9-2729-2009.

Bhartia, P. K., R. D. McPeters, L. E. Flynn, S. Taylor, N. A. Kramarova, S. Frith, B. Fisher, and M. DeLand (2013), Solar Backscatter UV (SBUV) total ozone and profile algorithm, *Atmos. Meas. Tech.*, *6*, 2533–2548, doi:10.5194/amt-6-2533-2013.

Butchart, N., and E. E. Remsberg (1986), The area of the stratospheric polar vortex as a diagnostic for tracer transport on an isentropic surface, *J. Atmos. Sci.*, *43*, 1319–1339.

Callis, L. B., M. Natarajan, J. D. Lambeth, and D. N. Baker (1998), Solar atmosphere coupling by electrons (SOLACE): 2. Calculated stratospheric effects of precipitating electrons, 1979–1988, *J. Geophys. Res.*, *103*, 28,421–28,438, doi:10.1029/98JD02407.

Crutzen, P. J., I. S. Isaaksen, and G. C. Reid (1975), Solar proton events: Stratospheric sources of nitric oxide, *Science*, *189*(4201), 457–459.

Damiani, A., M. Storini, M. Laurenza, and C. Rafanelli (2008), Solar particles effects on minor components of the polar atmosphere, *Ann. Geophys.*, *26*, 361–370.

Damiani, A., P. Diego, M. Storini, and C. Rafanelli (2010), The hydroxyl radical as an indicator of SEP fluxes in the high-latitude terrestrial atmosphere, *Adv. Space Res.*, *46*, 1225–1235.

De Zafra, R., and S. P. Smyshlyaev (2001), On the formation of $HNO_3$ in the Antarctic mid to upper stratosphere in winter, *J. Geophys. Res.*, *106*, 23,115–23,126, doi:10.1029/2000JD000314.

Du, Z. L. (2011), The correlation between solar and geomagnetic activity—Part 2: Long-term trends, *Ann. Geophys.*, *29*, 1341–1348.

Echer, E., W. D. Gonzalez, A. L. C. Gonzalez, A. Prestes, L. E. A. Vieira, A. Dal Lago, F. L. Guarnieri, and N. J. Schuch (2004), Long-term correlation between solar and geomagnetic activity, *J. Atmos. Sol. Terr. Phys.*, *66*(12), 1019–1025.

Farman, J. C., B. G. Gardiner, and J. D. Shanklin (1985), Large losses of total ozone in Antarctica reveal seasonal $CLO_x/NO_x$ interaction, *Nature*, *315*, 207–210.

Froidevaux, L., et al. (2008), Validation of Aura Microwave Limb Sounder stratospheric ozone measurements, *J. Geophys. Res.*, *113*, D15S20, doi:10.1029/2007JD008771.

Funke, B., et al. (2011), Composition changes after the "Halloween" solar proton event: The High-Energy Particle Precipitation in the Atmosphere (HEPPA) model versus MIPAS data intercomparison study, *Atmos. Chem. Phys.*, *11*(3), 9089–9139.

Funke, B., M. López-Puertas, L. Holt, C. E. Randall, G. P. Stiller, and T. von Clarmann (2014), Hemispheric distributions and interannual variability of $NO_y$ produced by energetic particle precipitation in 2002–2012, *J. Geophys. Res. Atmos.*, *119*, 13,565–13,582, doi:10.1002/2014JD022423.

Fytterer, T., M. G. Mlynczak, H. Nieder, K. Pérot, M. Sinnhuber, G. Stiller, and J. Urban (2015), Energetic particle induced intra-seasonal variability of ozone inside the Antarctic polar vortex observed in satellite data, *Atmos. Chem. Phys.*, *15*, 3327–3338, doi:10.5194/acp-15-3327-2015.

Hood, L., et al. (2015), Solar signals in CMIP-5 simulations: The ozone response, *Q. J. R. Meteorol. Soc.*, doi:10.1002/qj.2553.

Jackman, C. H., R. D. McPeters, G. J. Labow, E. L. Fleming, C. J. Praderas, and J. M. Russell (2001), Northern Hemisphere atmospheric effects due to the July 2000 solar proton event, *Geophys. Res. Lett.*, *28*, 2883–2886, doi:10.1029/2001GL013221.

Kodera, K., Y. Kuroda (2002), Dynamical response to the solar cycle: Winter stratopause and lower stratosphere, *J. Geophys. Res.*, *107*(D24), 4749, doi:10.1029/2002JD002224.

Kramarova, N. A., et al. (2013), Validation of ozone monthly zonal mean profiles obtained from the version 8.6 Solar Backscatter Ultraviolet algorithm, *Atmos. Chem. Phys.*, *13*, 6887–6905, doi:10.5194/acp-13-6887-2013.

Lean, J. L. (2014), Evolution of total atmospheric ozone from 1900 to 2100 estimated with statistical models, *J. Atmos. Sci.*, *71*, 1956–1984, doi:10.1175/JAS-D-13-052.1.

Livesey, N. J., et al. (2013), Earth Observing System (EOS) Aura Microwave Limb Sounder (MLS) version 3.3 and 3.4 level 2 data quality and description document, Rep. JPL D-33509, Version 3.3x/3.4x-1.1, Jet Propul. Lab., Calif. Inst. of Technol., Pasadena.

López-Puertas, M., B. Funke, S. Gil-López, T. von Clarmann, G. P. Stiller, M. Höpfner, S. Kellmann, H. Fischer, and C. H. Jackman (2005), Observation of $NO_x$ enhancements and ozone depletion in the Northern and Southern Hemispheres after the October–November 2003 solar proton events, *J. Geophys. Res.*, *110*, A09S43, doi:10.1029/2005JA011050.
Manney, G. L., et al. (2007), Solar occultation satellite data and derived meteorological products: Sampling issues and comparisons with Aura Microwave Limb Sounder, *J. Geophys. Res.*, *112*, D24S50, doi:10.1029/2007JD008709.
Miyagawa, K., I. Petropavlovskikh, R. D. Evans, C. Long, J. Wild, G. L. Manney, and W. H. Daffer (2014), Long-term changes in the upper stratospheric ozone at Syowa, Antarctica, *Atmos. Chem. Phys.*, *14*, 3945–3968, doi:10.5194/acp-14-3945-2014.
Orsolini, Y. J., J. Urban, and D. P. Murtagh (2009), Nitric acid in the stratosphere based on Odin observations from 2001 to 2009—Part 2: High-altitude polar enhancements, *Atmos. Chem. Phys.*, *9*, 7045–7052, doi:10.5194/acp-9-7045-2009.
Peck, E. D., C. E. Randall, V. L. Harvey, and D. R. Marsh (2015), Simulated solar cycle effects on the middle atmosphere: WACCM3 versus WACCM4, *J. Adv. Model. Earth Syst.*, doi:10.1002/2014MS000387.
Randall, C. E., et al. (2005), Stratospheric effects of energetic particle precipitation in 2003–2004, *Geophys. Res. Lett.*, *32*, L05802, doi:10.1029/2004GL022003.
Randall, C. E., V. L. Harvey, C. S. Singleton, S. M. Bailey, P. F. Bernath, M. Codrescu, H. Nakajima, and J. M. Russell, III (2007), Energetic particle precipitation effects on the Southern Hemisphere stratosphere in 1992–2005, *J. Geophys. Res.*, *112*, D08308, doi:10.1029/2006JD007696.
Rozanov, E., M. Callisto, T. Egorova, T. Peter, and W. Schmutz (2012), Influence of the precipitating energetic particles on atmospheric chemistry and climate, *Surv. Geophys.*, *33*, 483–501.
Santee, M. L., et al. (2007), Validation of the Aura Microwave Limb Sounder HNO3 measurements, *J. Geophys. Res.*, *112*, D24S40, doi:10.1029/2007JD008721.
Semeniuk, K., I. Usoskin, V. Fomichev, S. M. L. Melo, J. McConnell, and C. Fu (2011), Middle atmosphere response to the solar cycle in irradiance and ionizing particle precipitation, *Atmos. Chem. Phys.*, *11*, 5045–5077, doi:10.5194/acp-11-5045-2011.
Seppälä, A., P. T. Verronen, V. F. Sofieva, J. Tamminen, E. Kyrölä, C. J. Rodger, and M. A. Clilverd (2006), Destruction of the tertiary ozone maximum during a solar proton event, *Geophys. Res. Lett.*, *33*, L07804, doi:10.1029/2005GL025571.
Sinnhuber, M., B. Funke, T. von Clarmann, M. Lopez-Puertas, G. P. Stiller, and A. Seppälä (2014), Variability of $NO_x$ in the polar middle atmosphere from October 2003 to March 2004: Vertical transport vs. local production by energetic particles, *Atmos. Chem. Phys.*, *14*, 7681–7692, doi:10.5194/acp-14-7681-2014.
Solomon, S., D. W. Rusch, J. C. Gérard, G. C. Reid, and P. Crutzen (1981), The effect of particle precipitation events on the neutral and ion chemistry of the middle atmosphere: II odd hydrogen, *Planet. Space Sci.*, *29*, 885–892.
Stiller, G. P., et al. (2005), An enhanced HNO3 second maximum in the Antarctic midwinter upper stratosphere 2003, *J. Geophys. Res.*, *110*, D20303, doi:10.1029/2005JD006011.
Tiao, G., G. C. Reinsel, D. Xu, J. H. Pedrick, X. Zhu, A. J. Miller, J. J. DeLuisi, C. L. Mateer, and D. J. Wuebbles (1990), Effects of autocorrelation and temporal sampling schemes on estimates of trend and spatial correlation, *J. Geophys. Res.*, *95*, 20,507–20,517, doi:10.1029/JD095iD12p20507.
Tummon, F., et al. (2015), Intercomparison of vertically resolved merged satellite ozone data sets: Interannual variability and long-term trends, *Atmos. Chem. Phys.*, *15*, 3021–3043, doi:10.5194/acp-15-3021-2015.
Verronen, P. T., C. J. Rodger, M. A. Clilverd, and S. Wang (2011a), First evidence of mesospheric hydroxyl response to electron precipitation from the radiation belts, *J. Geophys. Res.*, *116*, D07307, doi:10.1029/2010JD014965.
Verronen, P. T., M. L. Santee, G. L. Manney, R. Lehmann, S.-M. Salmi, and A. Seppälä (2011b), Nitric acid enhancements in the mesosphere during the January 2005 and December 2006 solar proton events, *J. Geophys. Res.*, *116*, D17301, doi:10.1029/2011JD016075.

## Erratum

In the originally published version of this article, coauthor M. López Puertas (Instituto de Astrofísica de Andalucía, CSIC, Granada, Spain), was omitted from the author list. The omission has since been corrected, and this version may be considered the authoritative version of record.